Atmos. Chem. Phys. Discuss., 5, 7929–7964, 2005
www.atmos-chem-phys.org/acpd/5/7929/
SRef-ID: 1680-7375/acpd/2005-5-7929
European Geosciences Union

Atmospheric Chemistry and Physics Discussions

Intercomparison exercise between different radiative transfer models used for the interpretation of ground-based zenith-sky and multi-axis DOAS observations

F. Hendrick[1], M. Van Roozendael[1], A. Kylling[2,*], A. Petritoli[3], A. Rozanov[4], S. Sanghavi[5], R. Schofield[6,], C. von Friedeburg[5], T. Wagner[5], F. Wittrock[4], D. Fonteyn[1], and M. De Mazière[1]**

[1]Institut d'Aéronomie Spatiale de Belgique, Brussels, Belgium
[2]Norwegian Institute for Air Research, Kjeller, Norway
[3]Institute of Atmospheric Science and Climate, Bologna, Italy
[4]Institute of Environmental Physics, University of Bremen, Bremen, Germany
[5]Institute of Environmental Physics, University of Heidelberg, Heidelberg, Germany
[6]National Institute of Water and Atmospheric Research, Omakau, Central Otago, New Zealand

* now at: St. Olavs University Hospital, Trondheim, Norway
* now at: NOAA Aeronomy Laboratory, Boulder, Colorado, USA

Received: 30 June 2005 – Accepted: 23 August 2005 – Published: 2 September 2005

Correspondence to: F. Hendrick (franch@oma.be)

Abstract

We present the results of an intercomparison exercise between six different radiative transfer (RT) models carried out in the framework of QUILT, an EU funded project based on the exploitation of the Network for the Detection of Stratospheric Change (NDSC). RT modeling is an important step in the interpretation of Differential Optical Absorption Spectroscopy (DOAS) observations. It allows the conversion of the slant column densities (SCDs) into vertical column densities (VCDs) using calculated air mass factors (AMFs). The originality of our study resides in comparing SCD simulations in multi-axis (MAX) geometry (trace gases: NO_2 and HCHO) and in taking into account the photochemical enhancement for calculating SCDs of rapidly photolysing species (BrO, NO_2, and OClO) in zenith-sky geometry. Concerning the MAX simulations, good agreement is observed between the different models with the calculated NO_2 and HCHO SCDs differing by no more than 5% in the elevation and solar zenith angles (SZA) ranges investigated (5°–20° and 35°–85°, respectively). The impacts of aerosol scattering, ground albedo, and relative azimuth on MAX simulations have also been tested. Large discrepancies appear for the aerosol effect, suggesting differences between models in the treatment of the aerosol scattering. A better agreement is obtained in the case of the ground albedo and relative azimuth effects. In zenith-sky geometry, the different models agree generally well, especially below 90° SZA. At higher SZA, larger discrepancies are observed with relative difference values between 2% and 14% in some cases. All the initialization data and results have been made publicly available through the QUILT project web site (http://nadir.nilu.no/quilt/), enabling the testing of other RT codes designed for the calculation of SCDs/AMFs.

1 Introduction

Since the middle of the 1970s, stratospheric ozone and several trace gases directly or indirectly involved in the ozone depletion like NO_2, BrO, and OClO have been monitored from the ground using the Differential Optical Absorption Spectroscopy (DOAS)-technique (Platt, 1994). A significant part of this monitoring effort has been carried out through the framework of the Network for the Detection of Stratospheric Change (NDSC). The NDSC consists of about 20 sites combining complementary observations techniques distributed in five Primary Stations (Arctic, Alpine, Hawaii, New Zealand, and Antarctic) together with many globally distributed complementary sites. Network operations started in January 1991 and have provided a consistent, standardised set of long-term measurements of stratospheric and, more recently, tropospheric trace gases, particles, and physical parameters for detecting atmospheric change, validating space-borne sensors, and testing and improving multidimensional models of both the stratosphere and troposphere (further information at http://www.ndsc.ncep.noaa.gov/). Concerning the scattered sunlight DOAS instruments, they operated until recently almost only in zenith-sky geometry, thus probing mainly the altitude region corresponding to the stratosphere, especially at large solar zenith angles (SZAs). Over the last decade, new instruments pointing not only at zenith but also towards the horizon (off-axis geometry) have been developed (e.g., Heckel et al., 2005; Hönninger et al., 2004; Wagner et al., 2004; Wittrock et al., 2004). Pointing at an elevation angle close to the horizon provides sensitivity to the lowest absorption layers and therefore enables the measurement of tropospheric species. The Multi-AXis (MAX-) DOAS technique combines different elevation angles. Due to the variation of the light paths in the troposphere with the elevation angle, the different viewing directions have maximum sensitivity at different heights, thus providing some information on the vertical distribution of the absorber.

An important step in the interpretation of DOAS observations is the conversion of the slant column densities (SCDs) – which are the direct product of the DOAS analysis – into vertical column densities (VCDs) using calculated air mass factors (AMFs). The AMF represents the ratio of the effective optical path through the atmosphere to the vertical optical path and is given by the ratio SCD/VCD (Noxon et al., 1979; Solomon et al., 1987). In practice, AMFs are calculated using a radiative transfer (RT) model. In the

case of short lived species such as BrO, OClO, and NO_2, the calculation of SCDs and therefore AMFs is complicated by the variation of the concentration of these species along a given light path due to the fast diurnal variation of these radicals coupled to the local SZA variation along the light path (Fish et al., 1995). The so-called photochemical enhancement effect is taken into account by initializing RT models with a table containing the concentrations of the absorber for different heights and SZAs. This table is then interpolated to determine the trace gas concentration at the altitudes and local SZAs of the different scatter points considered along a given sun ray path. Such a concentration table is usually generated by running a stacked box photochemical model initialized with the output of a 3-D chemical transport model (CTM) corresponding to the day and location of interest. SCDs calculated by coupling a 3-D CTM to a photochemical box-/RT models interface can also be directly compared to observed SCDs. For example, Sinnhuber et al. (2002) compared ground-based zenith-sky UV-visible observations of BrO obtained at 11 sites with simulations from the 3-D CTM SLIMCAT (Chipperfield, 1999). The RT model used was based on the single scattering ray tracing scheme of Solomon et al. (1987). Recently, several groups have initiated AMF calculations in order to interpret MAX-DOAS measurements. Hönninger et al. (2004) have studied the behaviour of AMFs as a function of the solar zenith, elevation, and relative azimuth angles, ground albedo, and aerosol loading for several idealized trace gas profiles. For this purpose, they have used the RT model TRACY based on a Monte Carlo approach (von Friedeburg, 2003). This model has been also used by Wagner et al. (2004) to perform RT modeling for MAX-DOAS O_4 observations at different aerosol conditions. Sensitivity tests on O_4 AMFs were carried out by Wittrock et al. (2004) with SCIATRAN, a RT code based on a combined differential-integral approach involving the Picard iterative approximation (CDIPI) (Rozanov et al., 2000, 2001). In this work, SCIATRAN was also used to derive NO_2 profile information from MAX-DOAS observations. In Heckel et al. (2005), this model generated appropriate AMFs for the conversion of MAX-DOAS measurements of HCHO into VCDs. These examples show that RT modeling plays a central role in the interpretation of ground-based DOAS observations and that different

RT computation schemes are available for this purpose.

The QUILT (Quantification and Interpretation of Long-Term UV-Vis Observations of the Stratosphere) project is an EU funded project based on the exploitation of the NDSC and aimed at quantifying ozone loss and investigating its relation to active halogen and nitrogen species using the existing ground-based, satellite and balloon borne UV-visible data as well as 3-D atmospheric modelling tools. One of the tasks of this project has been to test the consistency between the different RT models existing within the consortium and used to interpret the ground-based and satellite DOAS data. This task has been achieved through several SCD simulations comparison tests performed using identical settings for all the models. Both ground zenith-sky (trace gases: BrO, NO_2, and OClO) and MAX geometries (trace gases: NO_2 and HCHO) have been considered for these tests, the photochemical enhancement being taken into account only in zenith-sky geometry.

Here we report on the results of this intercomparison exercise. It should be noted that our study does not address the issue of the absolute accuracy of the SCD calculations, the consistency between simulated and measured SCDs having already been tested in several papers (e.g., Sinnhuber et al., 2002; Tørnkvist et al., 2002). It can be considered to a certain extent as the continuation of Sarkissian et al. (1995) who calculated O_3 and NO_2 AMFs with different RT models in zenith-sky geometry but without taking into account the photochemical enhancement effect (use of a single profile for the initialization of the models). Our paper is divided into five parts. In Sect. 2, we describe the different RT models involved in the intercomparison exercise. The comparison tests in zenith-sky and MAX geometries are described in Sects. 3 and 4, respectively, and their corresponding results are discussed therein. Sects. 5 and 6 are dedicated to the impact of the aerosols and ground albedo on MAX simulations, respectively.

2 Description of the RT models

The groups contributing RT calculations to the intercomparison exercise were the remote sensing groups at the Universities of Bremen (UBRE) and Heidelberg (UHEI), Norwegian Institute for Air Research (NILU), Institute of Atmospheric Science and Climate (ISAC-CNR), National Institute of Water and Atmospheric Research (NIWA), and Institut d'Aéronomie Spatiale de Belgique (IASB). A summary of the characteristics of the models used by these groups is given in Table 1. From now on, each model will be referred to by the name of its corresponding group (in brackets here above). All the models include the possibility of taking into account the photochemical enhancement. The solution approaches to the RT equation (RTE) used in the different RT codes are as follows:

- The Finite Difference method (UBRE model): uses the integro-differential equations obtained by the expansion of the RTE in a Fourier cosine series in azimuth. The application of vertical and angular discretizations produces a matrix equation for each Fourier component which can be solved by using a recursion method (Lenoble, 1985; Rozanov et al., 2000 and 2001).
- The Discrete Ordinate method (NILU and IASB models): as in the Finite Difference method, the azimuth dependence of the radiation field is expressed as a Fourier cosine series in azimuth. However, the solution of the Fourier components is obtained in this case using a numerical quadrature scheme, allowing to replace the integrals by sums and thus reducing the RTE to the solution of a set of coupled linear first-order differential equations (Lenoble, 1985; Stamnes et al., 1988; Spurr, 2001).
- The backward Monte Carlo method (UHEI model): a photon emerges from a detector in an arbitrary line of sight direction and is followed in the backward direction along the path towards the sun. The various events which may happen

to the photon at various heights in the atmosphere are defined by suitable probability distributions. Random numbers decide on the occurrence of events. At the location of the last scattering event prior to leaving the atmosphere, the impinging radiance is calculated and weighted with the value of the scattering phase function and with the attenuation of the complete path. A large number of such random photon paths will reproduce the light contributing to the simulated measurement (von Friedeburg, 2003; Lenoble, 1985).

- Single scattering ray tracing (ISAC and NIWA models) method: in zenith-sky geometry, it consists of computing the attenuation from the sun through discrete spherical atmospheric shells to "points" where the light beams are scattered into the detector (Solomon et al., 1987).

3 Zenith-sky simulations of BrO, NO_2, and OClO SCDs including photochemical enhancement

3.1 Comparison test description

In this test, BrO, OClO, and NO_2 SCDs have been calculated in zenith-sky geometry in single scattering (SS) and when possible, in multiple scattering (MS) modes, taking into account the photochemical enhancement effect. The settings imposed for all models are summarized in Table 2. Color plots of the diurnal variation tables (concentration of BrO, OClO, and NO_2 as a function of the altitude and SZA) are shown in Figs. 1, 2, and 3, respectively. They are the output of the stacked box photochemical model PSCBOX (Errera and Fonteyn, 2001; Hendrick et al., 2000 and 2004) initialized with the 3-D-CTM SLIMCAT chemical and meteorological fields. Two scenarios have been considered: Harestua (60° N, Norway) at sunset in summer for NO_2 SCD calculations and Harestua at sunset under chlorine activated conditions for BrO and OClO. All calculations included absorption by O_3 and in the case of BrO and OClO, also the

absorption by NO_2.

3.2 Results

The results of the zenith-sky simulations of BrO, NO_2, and OClO SCDs are presented in Fig. 4. We first concentrate on the general behaviour of the simulated SCDs. Figure 4 shows that the impact of MS is more important for BrO than for NO_2, and for OClO, it is mostly significant at large SZA (>92°). The different behaviours of BrO and NO_2 regarding MS effects can be mainly attributed to the different wavelengths used for both calculations (352 nm for BrO and 422 nm for NO_2). In the case of OClO, the large impact of MS at SZA larger than ∼92° is related to the photochemistry of this species combined with geometrical considerations. Figure 2 shows that OClO is situated in the ∼17–22 km altitude range and only appears at SZA>92°. At these SZAs, the absorption due to OClO along a given line of sight occurs where the local SZA is the largest, i.e., near the vertical above the observing point. Given that, a significant part of the OClO layer is likely to be in the earth's shadow region and therefore can only be probed by multiply scattered light. This explains the large impact of MS on OClO SCDs in these conditions. The differences between the photochemical behaviours of BrO, NO_2, and OClO are also manifest from Fig. 4. BrO SCDs display a sharp decrease above ∼92° SZA (see Fig. 1), consistent with the rapid conversion of BrO into its night-time reservoirs (mostly BrCl in the present case) in the absence of sunlight. In contrast, the concentrations of OClO and NO_2 increase with the SZA (see Figs. 2 and 3, respectively), which explains the persistence of relatively large SCD values at corresponding SZAs, especially for MS mode.

Concerning the comparison of simulated SCDs, the relative differences between the results of the different models and the IASB ones arbitrarily taken as reference appear in the lower plots of Fig. 4 and a summary of the maximum difference values obtained is presented in Table 3. In SS mode, good agreement is observed below 90° SZA between the NIWA, IASB, NILU, and UBRE models: for the three species, the relative difference between the NIWA, NILU, and UBRE models and the IASB one (reference

model) is smaller than 1%. In the case of the ISAC-CNR model, simulated SCDs are systematically larger and the relative difference rises up to 4% for BrO, 5% for NO_2 and 7.5% for OClO. Above 90° SZA, agreement between the NIWA, IASB, UBRE, and NILU models is still very good with relative difference values smaller than 1.8% for BrO, 1.3% for NO_2, and 2.1% for OClO. A maximum spread between models of about 2% is a better agreement than the one obtained by Sarkissian et al. (1995) without taking into account the photochemical enhancement (from Sarkissian et al. (1995), the maximum spread values rise up to 13% for O_3 and 8% for NO_2 at 94° SZA). Concerning the ISAC-CNR simulations above 90° SZA, the discrepancies with the IASB model are larger than the ones observed for the NIWA and NILU models: the relative differences are smaller than 4% for BrO and rise up to 7.1% for NO_2, and 14.3% for OClO. Although these maximum relative difference values are consistent with those of Sarkissian et al. (1995), they suggest that the ISAC-CNR model differs from the other models in the way the optical thickness of each atmospheric shell is calculated. Sarkissian et al. (1995) investigated the influence of the different methods used to interpolate the concentration and to calculate the geometrical path in individual shells. They found that the impact of these parameters increases with increasing SZA and can reach 4% above 90° SZA. Since the photochemical enhancement is included in the present test, we cannot neglect the impact of differences in interpolating the tables of photochemical species concentrations. This effect is consistent with the observed increase of the relative differences between models with increasing SZA since the step between the SZA values corresponding to the concentration tables is increasing at large SZA. Concerning the calculations in MS mode, agreement below 90° SZA between the NILU, IASB, UBRE, and UHEI models is good since the relative differences with the IASB models are smaller than 4.4%. Above 90° SZA, slightly larger discrepancies are generally observed as in SS mode and the maximum relative differences with the IASB model rise up to 6.6% for the NILU model (obtained for OClO SCD calculations), 5.5% for the UHEI model (obtained for NO_2 SCD calculations), and 4.2% for the UBRE model (obtained for OClO SCD calculations). It should be noted that UHEI

OClO data are absent from the comparison. This is caused by the fact that too many photons (around 10^5) would have been required to calculate each SCD with sufficient accuracy and precision. In contrast to the NO_2 or BrO profile, the stratospheric OClO is usually confined to a layer of only a few kilometres thickness, and the concentration gradient is very high at its lower and upper ends (see Fig. 2). The Monte Carlo character of the UHEI model causes the scattering point altitude to vary around a given value. For a profile of the shape described, the SCD does react very sensitively to even small scattering altitude variation, i.e., a scattering location just below the profile yields a low SCD, while a slight shift upwards causes the photon to continue the flight on a slant path within the profile, leading to a sharp increase of the SCD. The Monte Carlo approach induced a variation of the scattering altitude, which in the case of OClO results in a strong variation of the SCD itself. This can only be overcome with a very large number of modelled photons, which causes the UHEI model to be inefficient for this specific kind of scenario. With the expected increase in computational power, this disadvantage is likely to become insignificant in a near future.

4 Multi-axis simulations of NO_2 and HCHO SCDs

4.1 Comparison test description

In contrast to the zenith-sky simulations, the photochemical enhancement has not been taken into account in the MAX simulations. The reason is that this effect becomes significant only during twilight, i.e. above 85° SZA, and we have limited our comparison in the 38°–85° SZA range because the sensitivity of the MAX-DOAS observations to the troposphere is largest during daytime, i.e. at small SZA. The NO_2 and HCHO profiles used for the initialization of the models are shown in Fig. 5. All calculations included absorption by O_3 and in the case of HCHO, also the absorption by NO_2. SCD simulations have been performed for 5°, 10°, and 20° of elevation above the horizon and for each elevation angle, four values of the azimuth angle of line of sight (AzLOS) have

been considered: 30°, 60°, 90°, and 120°. The AzLOS is the relative azimuth angle between the pointing direction of the instrument and the sun azimuth. The other settings appear in Table 4. Concerning the HCHO SCD calculations, the layer thickness in the altitude range where the concentration of this species changes rapidly with the altitude (0–3 km) has been fixed to 0.2 km instead of the 1 km thickness used in the case of NO_2, reducing interpolation effects. Only models enabling calculations in MS mode have been involved in this test since MS is the only acceptable scattering mode in MAX geometry (Wittrock et al., 2004). These models are: IASB, NILU, UBRE and UHEI.

4.2 Results

Figure 6 shows the results of NO_2 and HCHO SCD simulations for 5°, 10°, and 20° of elevation and 90° of AzLOS. A summary of the maximum difference values between the different models and the IASB one (again taken arbitrarily as reference model) is also presented in Table 5. The agreement between IASB, NILU, UBRE and UHEI is good: when comparing the results for both species over the whole SZA range and for all the elevation angles, the relative differences between the NILU, UBRE, and UHEI models and the IASB one are smaller than 5.1%. Concerning the UBRE model, it underestimates the IASB model results by maximum 4.5% for NO_2 and 5.1% for HCHO. The relative differences are also almost constant over the whole SZA range. This is in contrast with the relative differences between the UHEI and IASB models which show a SZA dependence, especially at low elevation angles: e.g., for NO_2 at 5° of elevation, the UHEI model overestimates the IASB one by 3% at 40° SZA and underestimates it by 3.6% at 85° SZA. However, with observed maximum relative difference of 3.8% for NO_2 and 4.5% for HCHO (see Table 5), the agreement between both models is good. As expected since they are both based on the UVspec/DISORT package, the NILU and the IASB models agree very well: for both NO_2 and HCHO, the relative difference between the results of both models is smaller than 1.3% over the entire SZA range and for all elevation angles.

The impact of the relative azimuth has been tested through the calculation of NO_2 and HCHO SCDs for different AzLOS values (30°, 60°, 90°, and 120°). Wittrock et al. (2004) have shown in their RT studies on O_4 AMF in MAX geometry that the AzLOS effect can be very large, especially for AzLOS pointing towards the sun (impact on O_4 AMF larger than 10% for AzLOS smaller than 90° compared to the 90° AzLOS case). The AzLOS effect on NO_2 SCDs is illustrated in Fig. 7 where the relative differences between the NO_2 SCDs at 30°, 60°, and 120° AzLOS and the SCDs at 90° AzLOS (reference) are plotted as a function of the SZA for 5° and 20° of elevation. As in Wittrock et al. (2004), the largest AzLOS effect is observed at small AzLOS and high elevation angle. However, its magnitude is significantly smaller than for O_4: about 7% on NO_2 SCDs at 50° SZA for 30° AzLOS and 20° of elevation instead of 45% for O_4 in similar conditions. It is also observed from Fig. 7 that the consistency between the IASB, NILU, UBRE, and UHEI models with respect to the impact of the AzLOS is reasonably good. In the case of HCHO (not shown here), the AzLOS effect is smaller by 1–2% than the one observed for NO_2.

5 Impact of aerosol scattering on multi-axis simulations of NO_2 and HCHO SCDs

The aerosols have a strong impact on MAX-DOAS observations (Wagner et al., 2004; Wittrock et al., 2004; and Heckel et al., 2005). The most important effect of the aerosol extinction is a reduction of the visibility of the atmosphere and thus a limitation by scattering of the light path of the lowest viewing directions, reducing the difference in tropospheric absorption path between the viewing directions. Given this effect and its impact on MAX-DOAS O_4 observations, Wagner et al. (2004) have also shown that O_4 observations can provide a new method for deriving information on atmospheric aerosols.

In the present study, MAX NO_2 and HCHO SCDs have been simulated with and without aerosol scattering in order to test the consistency between the different RT

models regarding the impact of the aerosols in this geometry. The aerosol extinction coefficient profiles used for initializing the models are shown in Fig. 8. They have been constructed from the aerosol model of Shettle (1989) included in the IASB and NILU RT models. Profiles of aerosol absorption coefficient and asymmetry factor have been also imposed in this test. The other settings are the same as the ones described in Sect. 4.1, except that HCHO and NO_2 SCDs have been calculated only for 90° of AzLOS.

Figure 9 shows the impact of the aerosol scattering on simulated MAX NO_2 and HCHO SCDs. Large discrepancies are observed between the UBRE and UHEI models and the IASB and NILU ones regarding the relative differences between simulations with and without aerosol scattering. In the case of HCHO, the impact of the aerosol scattering decreases and the agreement between the different models becomes better when the elevation angle increases. Similar features are observed for NO_2 but to a lesser extent. Figure 9 also shows that the impact of the aerosol scattering is smaller on HCHO than NO_2 SCDs: the relative differences between calculations with and without aerosol scattering are comprised for all models, elevation angles, and SZAs between −13% and +1.5% for HCHO and between −21% and +4% for NO_2. These discrepancies could not be resolved satisfactorily so far. Their origin is unlikely to be found in the aerosol settings since all models have been initialized with the same aerosol profiles (extinction and absorption coefficients and asymmetry factor). In order to progress further in our understanding of these persistent discrepancies, a thorough examination of individual aerosol routines and additional comparison tests appear to be needed, which is beyond the scope of the present intercomparison exercise. This issue, and more generally the impact of the aerosol scattering on MAX DOAS AMF simulations, will be addressed more thoroughly as part of a new exercise, currently led by the University of Heidelberg in the framework of the European Network of Excellence on Atmospheric Composition Change ACCENT.

6 Impact of ground albedo on multi-axis simulations of NO_2 and HCHO SCDs

Ground albedo has a significant impact on the radiative transfer close to the ground (Hönniger et al., 2004; Wittrock et al., 2004). It is particularly important to properly estimate this parameter for observational sites displaying large albedo changes depending on the season or viewing direction. The main effect of an increase of the albedo is an increase of the number of scattering events in the layers close to the surface, resulting in longer absorption paths at these altitudes and therefore to higher absolute AMFs. However, the difference in AMF between horizon and zenith-sky viewing directions is reduced, due to the fact that the enhancement of the optical path with increasing albedo is the largest for zenith-sky observations (Wittrock et al., 2004).

In order to test the consistency between the different RT models regarding the impact of the ground albedo in MAX geometry, NO_2 and HCHO SCDs have been simulated with ground albedo values fixed to 0 and 0.9. The other model settings are the same as those described in Sect. 4.1. As for the test on the impact of aerosol scattering, simulations have been performed only for 90° AzLOS.

Figure 10 illustrates the ground albedo effect on simulated MAX HCHO and NO_2 SCDs. The UBRE, NILU, and IASB models show excellent consistency with similar HCHO and NO_2 SCD increases being observed with the three models. An increase of the ground albedo value from 0.0 to 0.9 leads to an increase of the HCHO SCD of about 20% and 55% at 80° SZA for 5° and 20° of elevation, respectively, whereas the NO_2 SCD increases by 5% and 12% in the same conditions. The fact that the HCHO SCDs are more sensitive to the ground albedo is expected since for the present simulations, HCHO, in contrast to NO_2, is mostly located in the lower part of the troposphere (between 0 and 5 km). The corresponding increase of the SCD values are systematically larger using the UHEI model: 32% and 84% for HCHO SCDs, and 12% and 35% for NO_2 SCDs. This behaviour is likely to be attributed to the different concepts used in the Monte Carlo model as compared to the analytical codes and further tests would be needed to find out the detailed reasons of this.

7 Conclusions

In the present intercomparison exercise, we have tested the consistency between six RT models used for interpreting ground-based zenith-sky and MAX-DOAS observations in the QUILT EU project. In the context of this project based on the exploitation of the NDSC, the comparison and optimization of these RT models is of central importance in order to provide accurate time-series of ground-based DOAS observations. This study represents a step forward with respect to previously published work in that it compares RT models in MAX geometry and takes into account the photochemical enhancement effect for calculating SCDs of rapidly photolysing species in zenith-sky geometry.

Comparisons of NO_2 and HCHO SCDs in MAX geometry and multiple scattering mode show good agreement between all involved models: the calculated NO_2 and HCHO SCDs differ generally by no more than 5% in the SZA and elevation angle ranges investigated (35°–85° and 5°–20°, respectively). The impacts of the relative azimuth, aerosol scattering, and ground albedo on NO_2 and HCHO SCDs have been also quantitatively determined. As for O_4 in the Wittrock et al. (2004) study, the azimuth effect is found to be the largest at small AzLOS and high elevation angles. However, this effect is much smaller for NO_2 and HCHO than for O_4 (maximum differences relative to 90° AzLOS in the 30°–120° AzLOS range and for 20° of elevation rising up to 7% and 5% for NO_2 and HCHO SCDs, respectively, instead of 45% for O_4). The models have also shown reasonably good consistency concerning this effect. This is in contrast to the aerosol scattering effect for which large discrepancies still persist. Since all codes have been initialized in a common way, this result suggests that significant differences exist between the models regarding the treatment of the aerosol scattering. This issue, and more generally the impact of the aerosol scattering on the MAX DOAS AMF simulations, will be addressed more thoroughly as part of a new exercise, currently led by the University of Heidelberg in the framework of the European Network of Excellence ACCENT. Concerning the impact of the ground albedo, very good agreement has been

observed between the IASB, NILU, and UBRE models whereas the albedo effect is significantly larger using the UHEI model, which is based on a Monte Carlo approach. It should be noted that the conclusions drawn here on the levels of agreement between models in the different comparison tests depend on the assumptions made for the vertical profiles. In the case of NO_2 and HCHO, very different vertical profiles are indeed possible and could lead to different levels of agreement.

The comparisons of zenith-sky BrO, NO_2, and OClO SCDs calculated in both single and multiple scattering modes show good overall agreement to a level that is consistent and in some cases better than in the Sarkissian et al. (1995) work. In single scattering mode, the relative difference between the models is smaller than 1% below 90° SZA. In the case of the ISAC-CNR model, relative differences rising up to 7.5% have been observed in this SZA range. Above 90° SZA, agreement between the IASB, NILU, UBRE, and NIWA models is still very good with a maximum spread value of about 2%. Larger discrepancies have been observed with the ISAC-CNR model, especially in the OClO SCD calculations (relative difference with the IASB model up to 14%). These discrepancies could be partly due to differences in calculating the density in individual atmospheric shells. In multiple scattering mode, the differences between the NILU, UHEI, and UBRE models and the IASB one are smaller than 4.4% below 90° SZA for the three species. Above 90° SZA, slightly larger discrepancies have been observed with a maximum relative difference with the IASB model of about 6.5%. As in MAX geometry, the assumptions made on the vertical profiles used for the zenith-sky simulations can have an impact on the agreement observed between the models. This is particularly true for OClO, for which a small change in the vertical profiles could change the behaviour of the different models quite a bit.

All the initialization data (profiles and cross sections sets) and results of this intercomparison exercise have been gathered in a "RT model validation package" enabling the testing of other RT codes aiming to the calculation of SCDs/AMFs. This validation package has been made publicly available through the QUILT project web site (http://nadir.nilu.no/quilt/).

Acknowledgements. This research was financially supported by the European Commission (contract QUILT, EVK2-2000-00545) and the Belgian Federal Science Policy Office (contracts ESAC II EV/35/3A and MO/35/006 & 012). M. P. Chipperfield (University of Leeds) is acknowledged for providing us with the SLIMCAT data. We would like also to thank the coordinators of the QUILT EC project, B. Arlander and G. O. Braathen (NILU).

References

Barbe, A., Marché, P., Secroun, C., and Jouve, P.: Measurements of tropospheric and stratospheric H_2CO by an infrared high resolution technique, Geophys. Res. Lett., 6(6), 463–465, 1979.

Burrows, J. P., Dehn, A., Deters, B., Himmelmann, S., Richter, A., Voigt, S., and Orphal, J.: Atmospheric remote-sensing reference data from GOME: Part 1. Temperature dependent absorption cross sections of NO_2 in the 231–794 nm range, J. Quant. Spectrosc. Radiat, Transfer, 60, 1025–1031, 1998.

Burrows, J. P., Richter, A., Dehn, A., Deters, B., Himmelmann, S., Voigt, S., and Orphal, J.: Atmospheric remote-sensing reference data from GOME: Part 2. Temperature dependent absorption cross sections of O_3 in the 231–794 nm range, J. Quant. Spectrosc. Radiat. Transfer, 61, 509-517, 1999.

Cantrell, C. A., Davidson, J. A., McDaniel, A. H., Shetter, R. E., and Calvert, J. G.: Temperature-dependent formaldehyde cross sections in the near-ultraviolet region, J. Phys. Chem., 94, 3902–3908, 1990.

Chipperfield, M. P.: Multiannual simulations with a three-dimensional chemical transport model, J. Geophys. Res., 104(D1), 1781–1805, 1999.

Errera, Q. and Fonteyn, D.: Four-dimensional variational chemical assimilation of CRISTA stratospheric measurements, J. Geophys. Res., 106(D11), 12 253–12 265, 2001.

Ehhalt, D. H. and Tönnißen, A.: Hydrogen and carbon compounds in the stratosphere, Proceedings of the NATO Advanced Study Institute on Atmospheric Ozone: Its Variation and Human Influences, edited by: Aikin, A. C., Report No. FAA-EE-80-20, U.S. Federal Aviation Administration, 1979.

Fish, D. J., Jones, R. L., and Strong, E. K.: Midlatitude observations of the diurnal variation of stratospheric BrO, J. Geophys. Res., 100(D9), 18 863–18 871, 1995.

Hendrick, F., Mueller, R., Sinnhuber, B.-M., Bruns, M., Burrows, J. P., Chipperfield, M. P., Fonteyn, D., Richter, A., Van Roozendael, M., and Wittrock, F.: Simulation of BrO Diurnal Variation and BrO Slant Columns: Intercomparison Exercise Between Three Model Packages, Proceedings of the 5th European Workshop on Stratospheric Ozone, Saint Jean de Luz, France, 27 Sept.–1 Oct. 1999, Air Pollution Research Report no. 73, European Commission – DG XII, Brussels, 2000.

Hendrick, F., Barret, B., Van Roozendael, M., Boesch, H., Butz, A., De Mazière, M., Goutail, F., Hermans, C., Lambert, J.-C., Pfeilsticker, K., and Pommereau, J.-P.: Retrieval of nitrogen dioxide stratospheric profiles from ground-based zenith-sky UV-visible observations: validation of the technique through correlative comparisons, Atmos. Chem. Phys., 4, 2091–2106, 2004,
SRef-ID: 1680-7324/acp/2004-4-2091.

Heckel, A., Richter, A., Tarsu, T., Wittrock, F., Hak, C., Pundt, I., Junkermann, W., and Burrows, J. P.: MAX-DOAS measurements of formaldehyde in the Po-Valley, Atmos. Chem. Phys., 5, 909–918, 2005,
SRef-ID: 1680-7324/acp/2005-5-909.

Hönninger, G., Friedeburg, C. V., and Platt, U.: Multi Axis Differential Optical Absorption Spectroscopy (MAX-DOAS), Atmos. Chem. Phys., 4, 231–254, 2004,
SRef-ID: 1680-7324/acp/2004-4-231.

Lenoble, J.: Radiative Transfer in Scattering and Absorbing Atmospheres: Standard computational procedures, A. Deepak Publishing, Hampton, Virginia USA, 1985.

Mayer, B. and Kylling, A.: Technical note: The libRadtran software package for radiative transfer calculations – description and examples of use, Atmos. Chem. Phys., 5, 1855–1877, 2005,
SRef-ID: 1680-7324/acp/2005-5-1855.

Noxon, J. F., Whipple, E. C., and Hyde, R. S.: Stratospheric NO_2. 1. Observational method and behaviour at midlatitudes, J. Geophys. Res., 84, 5047–5076, 1979.

Petritoli, A., Ravegnani, F., Giovanelli, G., Bortoli, D., Bonafè, U., Kostadinov, I., and Oulanovsky, A.: Off-axis measurements of atmospheric trace gases by use of an airborne ultraviolet-visible spectrometer, Appl. Opt., 41(27), 5593–5599, 2002a.

Petritoli, A., Giovanelli, G., Kostadinov, I., Ravegnani, F., Bortoli, D., Bonasoni, P., Evangelisti, F., Bonafè, U., and Calzolari, F.: Tropospheric and stratospheric NO_2 amount deduced by slant column measurements at Mt. Cimone station, Adv. Space Res., 29(11), 1691–1695, 2002b.

Platt, U: Differential optical absorption spectroscopy (DOAS), in Air Monitoring by Spectroscopic Techniques, Chem. Anal. Ser., edited by: Sigrist, M. W., 127, 27–84, John Wiley, New York, 1994.

Rozanov, A., Rozanov, V.-V., and Burrows, J.-P.: Combined differential-integral approach for the radiation field computation in a spherical shell atmosphere: Nonlimb geometry, J. Geophys. Res., 105, D18, 22 937, 2000.

Rozanov, A., Rozanov, V.-V., and Burrows J.-P.: A numerical radiative transfer model for a spherical planetary atmosphere: combined differential-integral approach involving the Picard iterative approximation, J. Quant. Spectrosc. Radiat. Transfer, 69, 491, 2001.

Sarkissian, A., Roscoe, H. K., Fish, D., Van Roozendael, M., Gil, M., Chen, H. B., Wang, P., Pommereau, J.-P., and Lenoble, J.: Ozone and NO_2 air-mass factors for zenith-sky spectrometers: Intercomparison of calculations with different radiative transfer models, Geophys. Res. Lett., 22(9), 1113–1116, 1995.

Schofield, R.: The vertical distribution of atmospheric BrO from ground-based measurements, PhD thesis, University of Auckland, Auckland, 2003.

Schofield, R., Connor, B. J., Kreher, K., Johnston, P. V., and Rodgers, C. D.: The retrieval of profile and chemical information from ground-based UV-visible spectroscopic measurements, J. Quant. Spectrosc. Radiat. Transfer, 86, 115–131, 2004.

Shettle, E. P.: Models of aerosols, clouds, and precipitation for atmospheric propagation studies, AGARD Conference Proceedings No. 454: Atmospheric propagation in the UV, visible, IR and mm-region and related system aspects, 1989.

Sinnhuber, B.-M., Arlander, D. W., Bovensmann, H., Burrows, J. P., Chipperfield, M. P., Enell, C.-F., Frieß, U., Hendrick, F., Johnston, P. V., Jones, R. L., Kreher, K., Mohamed Tahrin, N., Müller, R., Pfeilsticker, K., Platt, U., Pommereau, J.-P., Pundt, I., Richter, A., South, A. M., Tørnkvist, K.K., Van Roozendael, M., Wagner, T., and Wittrock, F.: Comparison of measurements and model calculations of stratospheric bromine monoxide, J. Geophys. Res., 107(D19), 4398, doi:10.1029/2001JD000940, 2002.

Solomon, S., Schmeltekopf, A. L., and Sanders, R. W.: On the Interpretation of Zenith sky Absorption Measurements, J. Geophys. Res., 92(D7), 8311–8319, 1987.

Spurr, R. J. D.: Linearized Radiative Transfer Theory: A general discrete ordinate approach to the calculation of radiances and analytic weighting functions, with application to atmospheric remote sensing, PhD thesis, Technische Universiteit Eindhoven, 2001.

Stamnes, K., Tsay, S.-C., Wiscombe, W., and Jayaweera, K.: Numerically stable algorithm for

discrete-ordinate-method radiative transfer in multiple scattering and emitting layered media, Appl. Opt., 27, 2505–2509, 1988.

Tørnkvist, K. K., Arlander, D. W., and Sinnhuber, B.-M.: Ground-based UV measurements of BrO and OClO over Ny-Ålesund during Winter 1996 and 1997 and Andøya during Winter 1998/99, J. Atmos. Chem., 43(2), 75–106, 2002.

von Friedeburg, C.: Derivation of Trace Gas Information combining Differential Optical Absorption Spectroscopy with Radiative Transfer Modelling, PhD thesis, University of Heidelberg, 2003.

Wagner, T., Dix, B., Friedburg, C. v., Frieß, U., Sanghavi, S., Sinreich, R., and Platt, U.: MAX-DOAS O_4 measurements: A new technique to derive information on atmospheric aerosols-Principles and information content, J. Geophys. Res., 109, D22205, doi:10.1029/2004JD004904, 2004.

Wahner, A., Ravishankara, A. R., Sander, S. P., and Friedl, R.R.: Absorption cross-section of BrO between 312 and 385 nm at 298 and 223 K, Chem. Phys. Lett., 152, 507–512, 1988.

Wahner, A., Tyndall, G. Y., and Ravishankara, A. R.: Absorption cross-section for OClO as a function of temperature in the wavelength range from 240–490 nm, J. Phys. Chem., 91, 2735–2738, 1987.

Wittrock, F., Oetjen, H., Richter, A., Fietkau, S., Medeke, T., Rozanov, A., and Burrows, J. P.: MAX-DOAS measurements of atmospheric trace gases in Ny-Ålesund – Radiative transfer studies and their application, Atmos. Chem. Phys., 4, 955–966, 2004, SRef-ID: 1680-7324/acp/2004-4-955.

Table 1. Short description of the RT models involved in the intercomparison exercise. Note that both IASB and NILU models are based on the UVspec/DISORT package. However, they are not strictly identical since they have been adapted separately by each group in order to allow SCD/AMF calculations taking into account the photochemical enhancement.

Group	Model main features	Scattering mode(s)	Reference(s)
UBRE	SCIATRAN model: –Combining Differential-Integral approach using the Picard-Iterative approximation (CDIPI) –Treatment of MS in a full spherical geometry including refraction –Chemistry included (2-D array of profile variation with SZA) –Treatment for aerosol and cloud scattering, and ground albedo –Raman scattering included	SS+MS	Rozanov et al. (2000, 2001); Wittrock et al. (2004)
UHEI	TRACY model: –Backward Monte Carlo approach –Treatment of MS in a full spherical geometry including refraction –Chemistry included (2-D array of profile variation with SZA) –Treatments for aerosol and cloud scattering, and ground albedo –Raman scattering included	SS+MS (only MS in this study)	von Friedeburg (2003); Hönninger et al. (2004)
NILU and IASB	UVspec/DISORT package: –Discrete ordinate method –Chemistry included (2-D array of profile variation with SZA) –Treatment of MS and refraction in a pseudo-spherical geometry (direct beam only) –Treatment for aerosol and cloud scattering, and ground albedo	SS+MS	Mayer and Kylling (2005)
ISAC-CNR	AMEFCO model: –Single scattering model in a 2-D atmosphere (profile variation with SZA) –Treatment in full spherical geometry including refraction and aerosol scattering	SS	Petritoli et al. (2002a, b)
NIWA	–Single scattering model in a 2-D atmosphere (profile variation with SZA) –Treatment in full spherical geometry including refraction and aerosol scattering	SS	Schofield (2003); Schofield et al. (2004)

Table 2. Model settings for the comparison test in zenith-sky geometry. All the initialisation data are available on the QUILT web site (http://nadir.nilu.no/quilt/).

Altitude grid	0–120 km/1 km thick
Wavelength	352 nm (BrO) 368 nm (OClO) 422 nm (NO_2)
Diurnal variation table (see Figs. 1, 2, and 3)	From PSCBOX model
p, T profiles	From SLIMCAT 3-D-CTM; interpolation using AFGL 1976 outside the SLIMCAT altitude range
O_3 profile	From PSCBOX model; interpolation using AFGL 1976 outside the SLIMCAT altitude range
NO_2 profile (for BrO and OClO SCDs calculations)	From PSCBOX model; interpolation using AFGL 1976 outside the SLIMCAT altitude range
Mie scattering	Not included
Refraction	Not included
Cross sections sets	BrO: Wahner et al. (1988) OClO: Wahner et al. (1987) NO_2: Burrows et al. (1998) O_3: Burrows et al. (1999)
Ground albedo	0.20
Scattering mode	SS+if possible MS

Table 3. Maximum relative difference observed between the different RT models and the IASB one – arbitrarily taken as reference – for the comparison test in zenith-sky geometry. Note that the SS and MS models have been compared to the IASB model in SS and MS modes, respectively.

	BrO [%]	NO_2 [%]	OClO [%]
NILU SS	+1.0	+0.5	+2.1
ISAC SS	+4.1	+7.1	+14.3
NIWA SS	+1.5	+0.7	+1.6
UBRE SS	+1.8	+1.3	−1.4
NILU MS	+5.8	+2.7	+6.6
UHEI MS	−5.0	+5.5	–
UBRE MS	−1.0	−0.6	−4.2

Table 4. Model settings for the comparison test in MAX geometry. All the initialisation data are available on the QUILT web site (http://nadir.nilu.no/quilt/).

Altitude grid	NO_2: 0–120 km/1 km thick HCHO: 0–120 km/0.2 km thick between 0 and 3 km and 1 km thick above 3 km
Wavelength	356 nm (HCHO) 422 nm (NO_2)
p, T profiles	From SLIMCAT 3-D-CTM; interpolation using AFGL 1976 outside the SLIMCAT altitude range
O_3 profile	From PSCBOX model; interpolation using AFGL 1976 outside the SLIMCAT altitude range
NO_2 profile (for HCHO SCDs calculations)	From PSCBOX model; interpolation using AFGL 1976 outside the SLIMCAT altitude range
HCHO and NO_2 profiles (see Fig. 5)	HCHO: Barbe et al. (1979); Ehhalt and Tönnißen (1979) NO_2: from PSCBOX model
Mie scattering	Not included
Refraction	Not included
Cross sections sets	HCHO: Cantrell et al. (1990) NO_2: Burrows et al. (1998) O_3: Burrows et al. (1999)
Ground albedo	0.20
Elevation angle	5°, 10°, and 20°
Azimuth angle of line of sight	30°, 60°, 90°, and 120°
Scattering mode	MS

Table 5. Maximum relative difference observed between the different RT models and the IASB one – arbitrarily taken as reference – for the comparison test in MAX geometry.

		5° of elevation [%]	10° of elevation [%]	20° of elevation [%]
NILU MS	NO_2	−0.2	+0.2	+0.3
	HCHO	+1.0	+1.3	+1.1
UHEI MS	NO_2	−3.6	−3.2	−3.8
	HCHO	−3.0	−3.0	−4.5
UBRE MS	NO_2	−4.5	−3.7	−3.3
	HCHO	−5.0	−5.0	−5.1

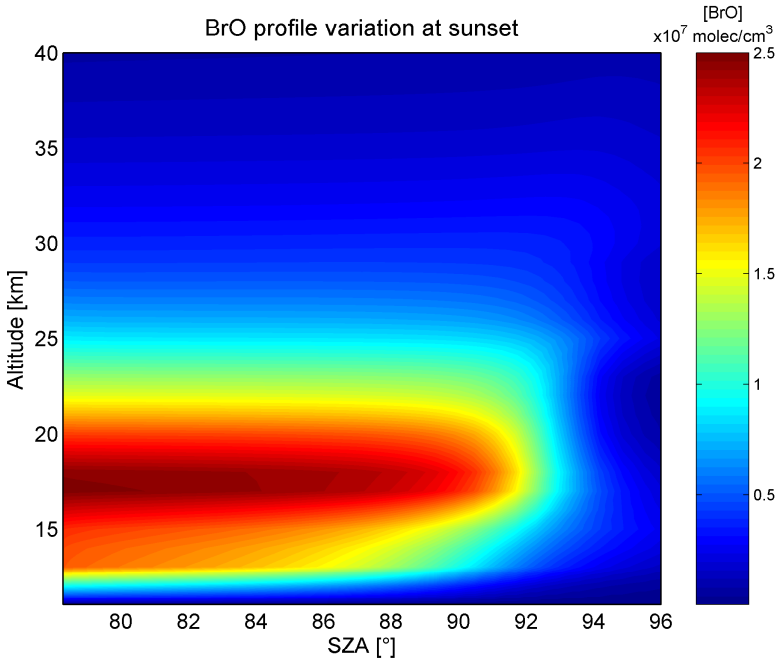

Fig. 1. Color plot of the BrO profiles table used to initialize the models in the comparison test in zenith-sky geometry. The variation of the BrO profiles as a function of the SZA has been calculated for Harestua (60° N, Norway) at sunset under chlorine activated conditions.

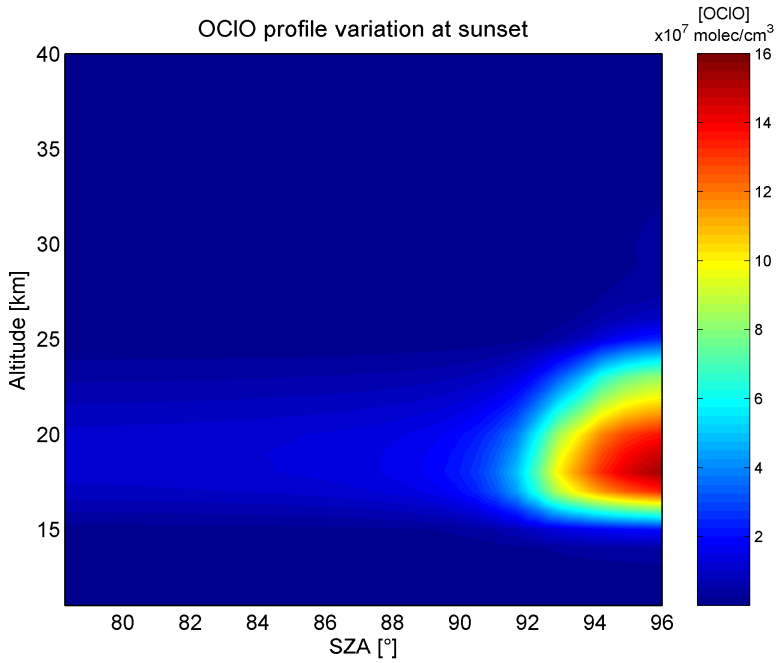

Fig. 2. Color plot of the OClO profiles table used to initialize the models in the comparison test in zenith-sky geometry. The variation of the OClO profiles as a function of the SZA has been calculated for Harestua (60° N, Norway) at sunset under chlorine activated conditions.

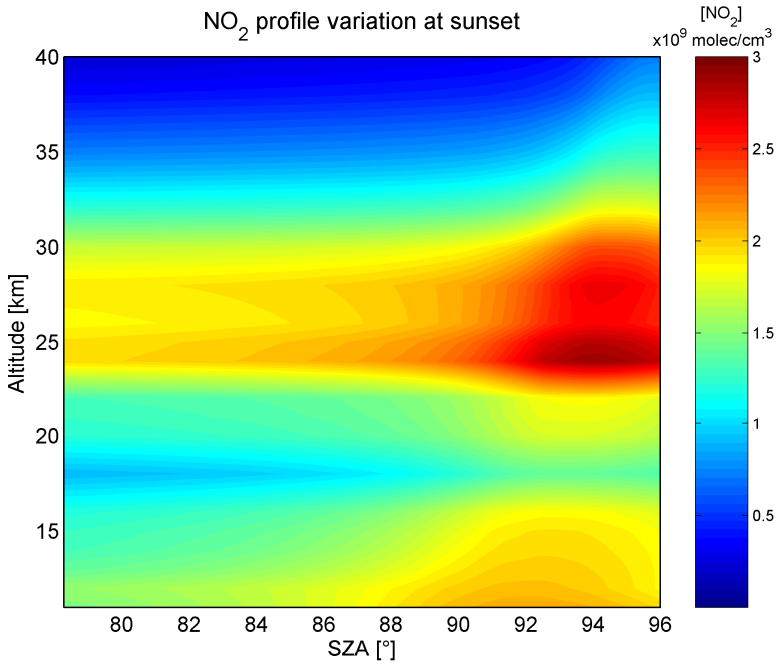

Fig. 3. Color plot of the NO_2 profiles table used to initialize the models in the comparison test in zenith-sky geometry. The variation of the NO_2 profiles as a function of the SZA has been calculated for Harestua (60° N, Norway) at sunset in summer.

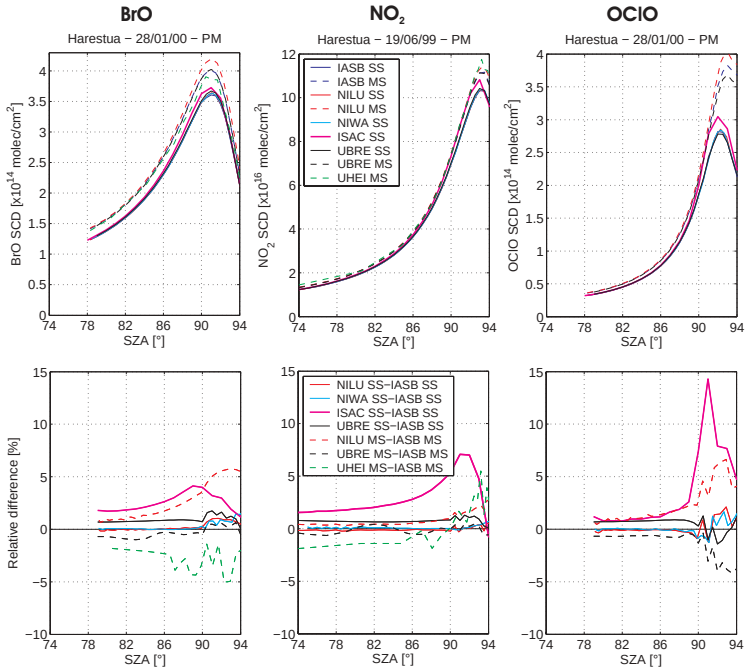

Fig. 4. Sunset BrO, NO_2, and OClO SCDs calculated in the comparison test in zenith-sky geometry. The upper plots correspond to the SCDs and the lower plots to the relative differences between the results from the different models and those from the IASB model arbitrarily chosen as reference. Solid and dashed lines correspond to calculations in SS and MS modes, respectively. Note that the UHEI OClO data are missing (see Sect. 3.2) and in the upper plots, the blue, red, and cyan solid lines corresponding to, respectively, the IASB, NILU, and NIWA SCD calculations in SS mode are almost superimposed.

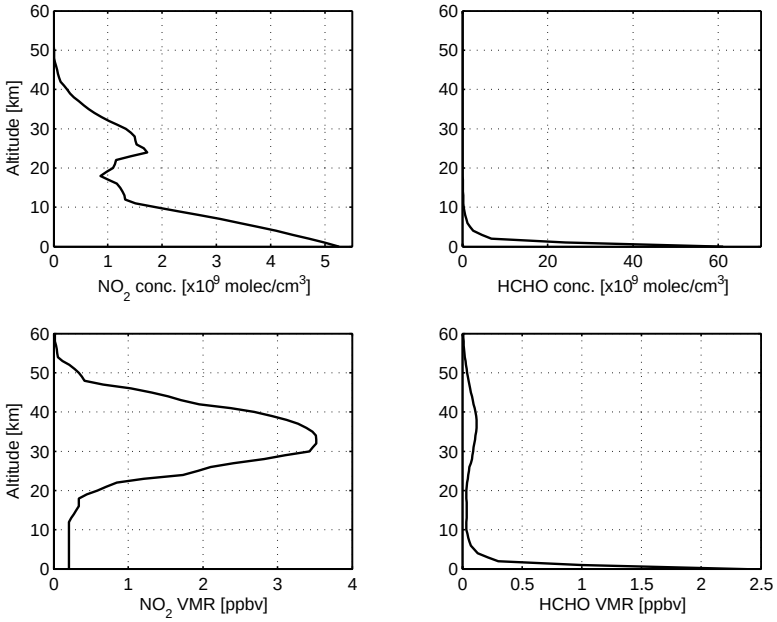

Fig. 5. NO_2 (left) and HCHO (right) profiles in concentration (upper plots) and VMR (lower plots) used to initialize the RT models in the comparison tests in MAX geometry.

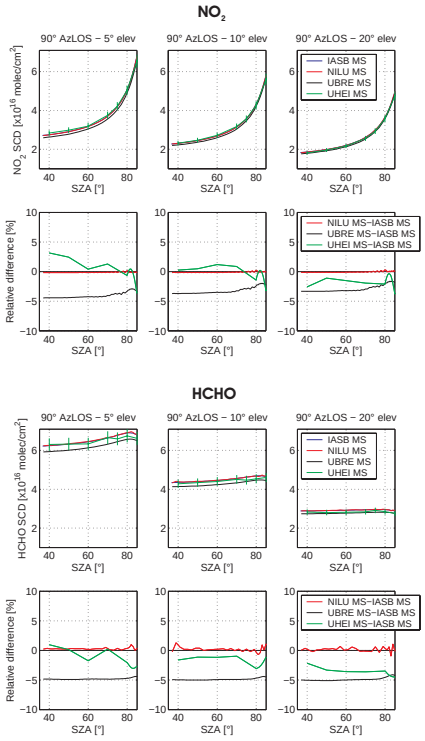

Fig. 6. NO_2 and HCHO SCDs calculated in MS mode in the comparison test in MAX geometry. For each species, the upper plots correspond to the SCDs and the lower plots to the relative differences between the different models and the IASB one arbitrarily chosen as reference. Results for 90° AzLOS and for 5°, 10°, and 20° of elevation are plotted here.

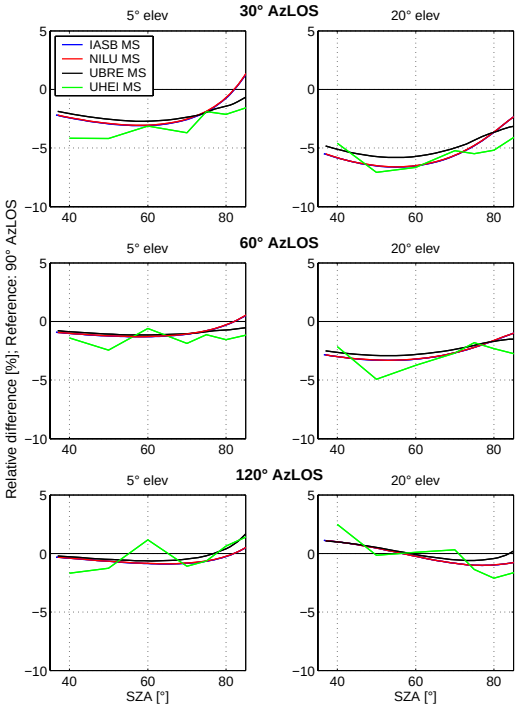

Fig. 7. Impact of the relative azimuth on the NO_2 SCDs calculated in MAX geometry. Here are plotted the relative differences between the NO_2 SCDs calculated at 30° (upper plots), 60° (middle plots), and 120° (lower plots) AzLOS and those calculated at 90° AzLOS (reference case). Left and right plots correspond to results for 5° and 20° of elevation, respectively. Note that the IASB blue lines are superimposed to the NILU red lines.

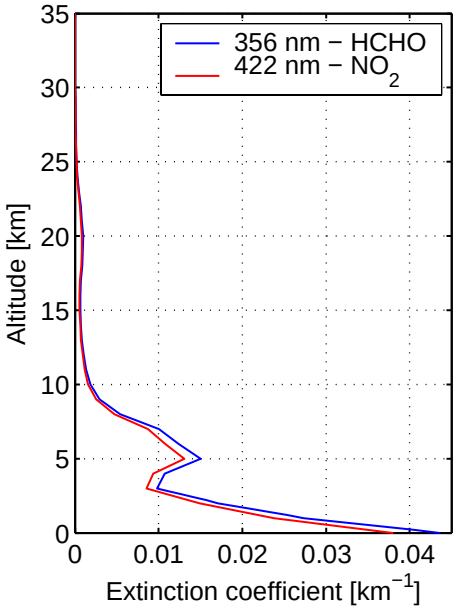

Fig. 8. Profiles of the aerosol extinction coefficient at 356 nm and 422 nm used for testing the impact of the aerosols on MAX simulations of HCHO and NO_2 SCDs, respectively.

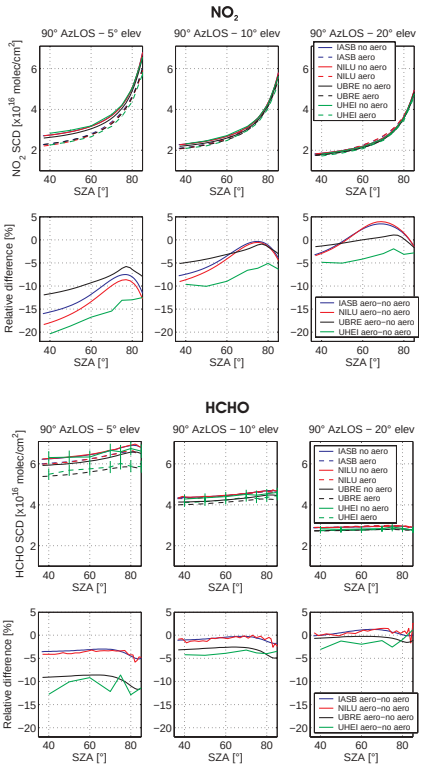

Fig. 9. Impact of the aerosol scattering on simulated MAX NO_2 and HCHO SCDs. For each species, the upper plots correspond to the SCDs and the lower plots to the relative differences between SCDs calculated with and without aerosol scattering (reference: without aerosol scattering). Results for 90° AzLOS and for 5°, 10°, and 20° of elevation are plotted here.

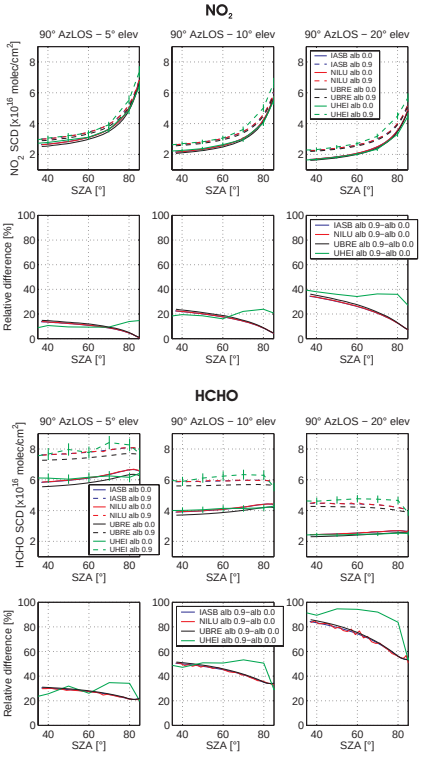

Fig. 10. Impact of the ground albedo on simulated MAX NO_2 and HCHO SCDs. For each species, the upper plots correspond to the SCDs and the lower plots to the relative differences between SCDs calculated with ground albedo values of 0.9 and 0.0 (reference: albedo=0.0). Results for 5°, 10°, and 20° of elevation and 90° AzLOS are plotted here.